Inorganic Chemistry
Article

Inorg. Chem. **2010**, *49*, 9125–9135 **9125**
DOI: 10.1021/ic100460w

Face-Sharing Heterotrinuclear $M^{II}-Ln^{III}-M^{II}$ (M = Mn, Fe, Co, Zn; Ln = La, Gd, Tb, Dy) Complexes: Synthesis, Structures, and Magnetic Properties

Tomoka Yamaguchi,[†] Jean-Pierre Costes,*[,‡] Yukana Kishima,[†] Masaaki Kojima,*[,†] Yukinari Sunatsuki,[†] Nicolas Bréfuel,[‡] Jean-Pierre Tuchagues,[‡] Laure Vendier,[‡] and Wolfgang Wernsdorfer[§]

[†]*Department of Chemistry, Faculty of Science, Okayama University, Tsushima-naka 3-1-1, Okayama 700-8530, Japan,* [‡]*Laboratoire de Chimie de Coordination du CNRS, UPR 8241, liée par conventions à l'Université Paul Sabatier et à l'Institut National Polytechnique de Toulouse, 205 route de Narbonne, 31077 Toulouse Cedex, France, and* [§]*Institut Néel, CNRS & Université J. Fourier, BP 166, 38042 GRENOBLE Cedex 9, France*

Received March 9, 2010

Trinuclear linear 3d−4f−3d complexes (3d = Mn^{II}, Fe^{II}, Co^{II}, Zn^{II} and 4f = La^{III}, Gd^{III}, Tb^{III}, Dy^{III}) were prepared by using a tripodal nonadentate Schiff base ligand, *N,N′,N″*-tris(2-hydroxy-3-methoxybenzilidene)-2-(aminomethyl)-2-methyl-1,3-propanediamine. The structural determinations showed that in these complexes two distorted trigonal prismatic transition metal complexes of identical chirality are assembled through 4f cations. The Mn and Fe entities crystallize in the chiral space group $P2_12_12_1$ as pure enantiomers; the cobalt complexes exhibit a less straightforward behavior. All Mn, Fe, and Co complexes experience $M^{II}-Ln^{III}$ ferromagnetic interactions. The Mn−Gd interaction is weak (0.08 cm^{-1}) in comparison to the Fe−Gd (0.69 cm^{-1}) and Co−Gd (0.52 cm^{-1}) ones while the single ion zero field splitting (ZFS) term *D* is larger for the Fe complexes (5.7 cm^{-1}) than for the cobalt ones. The cobalt complexes behave as single-molecules magnets (SMMs) with large magnetization hysteresis loops, as a consequence of the particularly slow magnetic relaxation characterizing these trinuclear molecules. Such large hysteresis loops, which are observed for the first time in Co-Ln complexes, confirm that quantum tunnelling of the magnetization does not operate in the Co−Gd−Co complex.

Introduction

The first 3d−4f complexes derived from Schiff base ligands involved Cu^{II} and Gd^{III} ions, because of the frequent occurrence of ferromagnetic coupling between these ions and the possibility of using an isotropic Hamiltonian to quantify the interaction.[1−3] It has been emphasized that most of these complexes have a coordination geometry close to C_{2v} symmetry, with the metal ions linked by two phenoxo bridges.[4] This remark is also true for the few examples of complexes involving Ni^{II},[5] Co^{II},[6] or Fe^{II} [7] ions. Recently, we have reacted a triamine 1,1,1-tris(aminomethyl)ethane (tame) with salicylaldehyde to obtain a tripodal ligand[8] (H_3L' = 1,1,1-tris-[(salicylideneamino)methyl]ethane) that is able to chelate Ni^{II} or Zn^{II} ions to yield approximately octahedral complexes.[9] Further reaction with gadolinium ions according to the "complex as ligand" strategy allowed us to control the nuclearity of the Ni−Gd complexes by selecting additional ligands on the Gd^{III} ions.[8−10] In this way, di-, tri-, and tetranuclear complexes could be isolated.[8] To prevent the additional ligands to enter the Ln^{III} coordination sphere, we synthesized a new tripodal ligand, starting from tame and *o*-vanillin, and expecting that the methoxy groups would be able to prevent auxiliary ligands from entering the coordination sphere of the central Ln ion. In addition, this strategy would have the advantage of yielding linear face-sharing complexes. Furthermore, in a face-sharing complex, both $d_{x^2-y^2}$ and d_{z^2} e_g orbitals are involved in bridging. This situation,

*To whom correspondence should be addressed. E-mail: costes@lcc-toulouse.fr (J.-P.C.). Fax: 33 (0)5 61 55 30 03; E-mail: kojima@cc.okayama-u.ac.jp (J.-P.C.).

(1) Benelli, C.; Gatteschi, D. *Chem. Rev.* **2002**, *102*, 2369–2387.
(2) Sakamoto, M.; Manseki, K.; Okawa, H. *Coord. Chem. Rev.* **2001**, *219−221*, 379–414.
(3) Costes, J. P.; Dahan, F.; Dupuis, A.; Laurent, J. P. *Inorg. Chem.* **2000**, *39*, 165–168.
(4) Paulovic, J.; Cimpoesu, F.; Ferbinteanu, M.; Hirao, K. *J. Am. Chem. Soc.* **2004**, *126*, 3321–3331.
(5) Costes, J. P.; Dahan, F.; Dupuis, A.; Laurent, J. P. *Inorg. Chem.* **1997**, *36*, 4284–4286.
(6) Costes, J. P.; Dahan, F.; García-Tojal, J. *Chem.—Eur. J.* **2002**, *8*, 5430–5434.
(7) Costes, J. P.; Clemente-Juan, J. M.; Dahan, F.; Dumestre, F.; Tuchagues, J. P. *Inorg. Chem.* **2002**, *41*, 2886–2891.
(8) Yamaguchi, T.; Sunatsuki, Y.; Kojima, M.; Akashi, H.; Tsuchimoto, M.; Re, N.; Osa, S.; Matsumoto, N. *Chem. Commun.* **2004**, 1048–1049.
(9) Yamaguchi, T.; Sunatsuki, Y.; Ishida *Acta Crystallogr.* **2008**, *C64*, m156–m160.
(10) (a) Yamaguchi, T.; Sunatsuki, Y.; Ishida, H.; Kojima, M.; Akashi, H.; Re, N.; Matsumoto, N.; Pochaba, A.; Mroziński, J. *Bull. Chem. Soc. Jpn.* **2008**, *81*, 598–605. (b) Yamaguchi, T.; Sunatsuki, Y.; Ishida, H.; Kojima, M.; Akashi, H.; Re, N.; Matsumoto, N.; Pochaba, A.; Mroziński, J. *Inorg. Chem.* **2008**, *47*, 5736–5745.

Published on Web 05/06/2010

different from the one in a planar edge-sharing complex, would allow an interesting comparison between these two types of complexes and should bring additional information about the 3d−4f magnetic interactions. Because tripodal ligands favor an octahedral environment, we have used Co^{II} and Fe^{II} ions in our syntheses to take advantage of the anisotropy of the 3d or 4f ions, or both ions in the same complex. We have also extended our study to the Mn^{II} ions, Mn^{II}−Ln complexes with Schiff base ligands being very scarce.[11] The SMMs based on lanthanide ions, which involve 4f−2p, 4f−3d or pure 4f polynuclear systems, have been recently reviewed.[12] The 3d−4f systems present two main interests. First, the 3d−4f magnetic interaction is most often ferromagnetic,[13] thus inducing large ground spin-states (large S values), and second, lanthanide ions such as Tb or Dy bring a large uniaxial magnetic anisotropy. According to the anisotropy Hamiltonian $H = D S_{Tz}^2 + E(S_{Tx}^2 - S_{Ty}^2)$,[14] the D term must be large and negative while the E term has to be small. The first 3d−4f SMM was a tetranuclear Cu_2−Tb_2 complex.[15] After being mainly based on copper as 3d ion, systems including Fe^{II}, Fe^{III}, Mn^{II}, Mn^{III} as 3d ions were studied.[12] There are very few examples involving Co^{II} ions.[16] Because Co^{II} ions are anisotropic, they can be associated to the isotropic gadolinium ion ($S = 7/2$), as reported for a few examples.[16a] The present contribution describes the syntheses and magnetic properties of 13 trinuclear [LMLnML]X complexes, L being the trideprotonated form of *N,N′,N″*-tris-(2-hydroxy-3-methoxybenzilidene)-2-(aminomethyl)-2-methyl-1,3-propanediamine, M = Mn^{II}, Fe^{II}, Co^{II}, Zn^{II} and Ln = La^{III}, Gd^{III}, Tb^{III}, Dy^{III}, among which anisotropy can be brought by the 3d ions, the 4f ions, and also by both the 3d and 4f ions. The structural determinations of nine of these complexes are reported.

Experimental Section

Materials. The metal salts, $Co(CH_3COO)_2 \cdot 4H_2O$, $Mn(CH_3COO)_2 \cdot 4H_2O$, $Fe(ClO_4)_2 \cdot 6H_2O$, $Zn(CH_3COO)_2 \cdot 2H_2O$, $La(NO_3)_3 \cdot 5H_2O$, $Gd(NO_3)_3 \cdot 5H_2O$, $Tb(NO_3)_3 \cdot 5H_2O$, $Dy(NO_3)_3 \cdot 5H_2O$, (Aldrich) were used as purchased. High-grade solvents were used for preparing the complexes.

Ligand. *N,N′,N″*-tris(2-hydroxy-3-methoxybenzilidene)-2-(aminomethyl)-2-methyl-1,3-propanediamine, **H_3L**.

The triamine 1,1,1-tris(aminomethyl)ethane) hydrochloride (tame·3HCl) was prepared as described previously.[17] To the triamine hydrochloride (0.113 g, 0.5 mmol) dissolved in water (20 mL) was added first a water solution (20 mL) of NaOH (0.06 g, 1.5 mmol) followed by a dichloromethane solution (40 mL) containing *o*-vanillin (0.228 g, 1.5 mmol). The mixture was stirred vigorously for 2 h and transferred into a separating funnel. The dichloromethane layer was collected and dried. The solvent was removed to yield an orange-brown oil that was deoxygenated and used for preparation of the complexes in a glovebox. ^{1}H NMR (250 MHz, dimethyl sulfoxide−d_6): δ 1.16 (s, 3H, CH_3), 3.72 (s, 6H, CH_2), 3.90 (s, 9H, CH_3), 6.94 (t, J = 8 Hz, 3H, H5), 7.14 (d, J = 8 Hz, 3H, H4), 7.36 (d, J = 8 Hz, 3H, H6), 8.67 (s, 3H, HC=N), 13.79 (s, 3H, OH).

Complexes. The 13 complexes were prepared and isolated through the same experimental procedure, as described for complex **1**. Using the appropriate metal salt yielded the desired complexes. The reactions and preparation of the samples for physical measurements were carried out in a purified nitrogen atmosphere within a glovebox (Vacuum Atmospheres H.E.43.2) equipped with a dry train (Jahan EVAC 7).

Caution! *Because of their explosive character, perchlorate salts should be handled with care and in very low amounts.*

[LCoGdCoL]NO_3, 1. The ligand (0.5 mmol) was diluted in dry methanol (20 mL) inside the glovebox. Then cobalt acetate (0.124 g, 0.5 mmol) followed by gadolinium nitrate (0.112 g, 0.25 mmol) were added to the homogeneous solution which was stirred, yielding a clear solution. The solution was filtered and kept undisturbed during a few days, until orange crystals formed, which were isolated by filtration and dried inside the glovebox. Yield: 0.24 g (36%). Anal. Calcd for $C_{58}H_{60}Co_2GdN_7O_{15}$: C, 50.8; H, 4.4; N, 7.2. Found: C, 50.7; H, 4.3; N, 7.1. IR (KBr): ν(C=N) 1622 cm^{-1}, $\nu(NO_3)$ 1384 cm^{-1}.

[LCoTbCoL]NO_3, 2. Yield: 0.21 g (30%). Anal. Calcd for $C_{58}H_{60}Co_2N_7O_{15}Tb$: C, 50.8; H, 4.4; N, 7.2. Found: C, 49.9; H, 4.2; N, 6.9. IR (KBr): ν(C=N) 1622 cm^{-1}, $\nu(NO_3)$ 1384 cm^{-1}.

[LCoDyCoL]$NO_3 \cdot CH_3OH$, 3. Yield: 0.22 g (31%). Anal. Calcd for $C_{59}H_{64}Co_2DyN_7O_{16}$: C, 50.3; H, 4.6; N, 7.0. Found: C, 50.2; H, 4.5; N, 6.8. IR (KBr): ν(C=N) 1622 cm^{-1}, $\nu(NO_3)$ 1383 cm^{-1}.

[LCoLaCoL]$NO_3 \cdot CH_3OH$, 4. Yield: 0.23 g (33%). Anal. Calcd for $C_{59}H_{64}Co_2LaN_7O_{16}$: C, 51.2; H, 4.7; N, 7.1. Found: C, 51.0; H, 4.5; N, 7.0. IR (KBr): ν(C=N) 1619 cm^{-1}, $\nu(NO_3)$ 1384 cm^{-1}.

[LMnGdMnL]NO_3, 5. Yield: 0.26 g (38%). Anal. Calcd for $C_{58}H_{60}GdMn_2N_7O_{15}$: C, 51.1; H, 4.4; N, 7.2. Found: C, 51.0; H, 4.2; N, 7.1. IR (KBr): ν(C=N) 1623 cm^{-1}, $\nu(NO_3)$ 1384 cm^{-1}.

[LMnTbMnL]NO_3, 6. Yield: 0.24 g (35%). Anal. Calcd for $C_{58}H_{60}Mn_2N_7O_{15}Tb$: C, 51.1; H, 4.4; N, 7.2. Found: C, 50.5; H, 4.3; N, 7.0. IR (KBr): ν(C=N) 1619 cm^{-1}, $\nu(NO_3)$ 1384 cm^{-1}.

[LMnDyMnL]$NO_3 \cdot CH_3OH$, 7. Yield: 0.24 g (34%). Anal. Calcd for $C_{59}H_{64}DyMn_2N_7O_{16}$: C, 50.6; H, 4.6; N, 7.0. Found: C, 50.4; H, 4.3; N, 7.0. IR (KBr): ν(C=N) 1623 cm^{-1}, $\nu(NO_3)$ 1384 cm^{-1}.

[LFeGdFeL]ClO_4, 8. Yield: 0.27 g (38%). Anal. Calcd for $C_{58}H_{60}ClFe_2GdN_6O_{16}$: C, 49.7; H, 4.3; N, 6.0. Found: C, 49.5; H, 4.2; N, 5.9. IR (KBr): ν(C=N) 1617 cm^{-1}, ν_3, $\nu_4(ClO_4)$ 1083, 622 cm^{-1}.

[LFeTbFeL]$ClO_4 \cdot CH_3OH$, 9. Yield: 0.28 g (39%). Anal. Calcd for $C_{59}H_{64}ClFe_2N_6O_{17}Tb$: C, 49.4; H, 4.5; N, 5.9. Found: C, 49.3; H, 4.4; N, 5.8. IR (KBr): ν(C=N) 1617 cm^{-1}, ν_3, $\nu_4(ClO_4)$ 1083, 622 cm^{-1}.

[LFeDyFeL]$ClO_4 \cdot CH_3OH$, 10. Yield: 0.26 g (36%). Anal. Calcd for $C_{59}H_{64}ClDyFe_2N_6O_{17}$: C, 49.2; H, 4.5; N, 5.8. Found: C, 48.9; H, 4.4; N, 5.6. IR (KBr): ν(C=N) 1619 cm^{-1}, ν_3, $\nu_4(ClO_4)$ 1083, 622 cm^{-1}.

[LFeLaFeL]$ClO_4 \cdot CH_3OH$, 11. Yield: 0.23 g (33%).Anal. Calcd for $C_{59}H_{64}ClFe_2LaN_6O_{17}$: C, 50.1; H, 4.6; N, 5.9. Found: C, 49.9; H, 4.4; N, 5.7. IR (KBr): ν(C=N) 1615 cm^{-1}, ν_3, $\nu_4(ClO_4)$ 1083, 622 cm^{-1}.

[LZnTbZnL]$NO_3 \cdot 3H_2O$, 12. Yield: 0.25 g (35%). Anal. Calcd for $C_{58}H_{66}N_7O_{18}TbZn_2$: C, 48.4; H, 4.6; N, 6.8. Found: C, 48.3; H, 4.5; N, 6.7. IR (KBr): ν(C=N) 1623 cm^{-1}, $\nu(NO_3)$ 1384 cm^{-1}.

(11) Costes, J. P.; Garcia-Tojal, J.; Tuchagues, J. P.; Vendier, L. *Eur. J. Inorg. Chem.* **2009**, 3801–3806.
(12) Sessoli, R.; Powell, A. K. *Coord. Chem. Rev.* **2009**, *253*, 2328–2341.
(13) (a) Sutter, J.-P.; Kahn, M. L. In *Magnetism: Molecules to Materials*; Miller, J. S., Drillon, M., Eds.; Wiley-VCH: Weinheim, Germany, 2005; Vol. *V*, pp 161−187. (b) Andruh, M.; Costes, J. P.; Diaz, C.; Gao, S. *Inorg. Chem.* **2009**, *48*, 3342–3359. (c) Sanz, J. L.; Ruiz, R.; Gleizes, A.; Lloret, F.; Faus, J.; Julve, M.; Borras-Almenar, J. J.; Journaux, Y. *Inorg. Chem.* **1996**, *35*, 7384–7393.
(14) (a) Gatteschi, D.; Sessoli, R. *Angew. Chem., Int. Ed.* **2003**, *42*, 268–297. (b) Wernsdorfer, W. *Adv. Chem. Phys.* **2001**, *118*, 99–190.
(15) Osa, S.; Kido, T.; Matsumoto, N.; Re, N.; Pochaba, A. *J. Am. Chem. Soc.* **2004**, *126*, 420–421.
(16) (a) Chandrasekhar, V.; Murugesu Pandian, B.; Azhakar, R.; Vittal, J. J.; Clérac, R. *Inorg. Chem.* **2007**, *46*, 5140–5142. (b) Huang, Y. G.; Wang, X. T.; Jiang, F. L.; Gao, S.; Wu, M. Y.; Gao, Q.; Wei, W.; Hong, M. C. *Chem.—Eur. J.* **2008**, *14*, 10340–10347.
(17) Fleischer, E. B.; Gebala, A. E.; Levey, A.; Tasker, P. A. *J. Org. Chem.* **1971**, *36*, 3042–3044.

[LZnDyZnL]$NO_3 \cdot 2H_2O$, 13. Yield: 0.23 g (33%). Anal. Calcd for $C_{58}H_{64}DyN_7O_{17}Zn_2$: C, 48.9; H, 4.5; N, 6.9. Found: C, 48.8; H, 4.5; N, 6.7. IR (KBr): ν(C=N) 1623 cm^{-1}, $\nu(NO_3)$ 1384 cm^{-1}.

Physical Measurements. C, H, and N elemental analyses were carried out at the Laboratoire de Chimie de Coordination Microanalytical Laboratory in Toulouse, France. IR spectra were recorded on a GX system 2000 Perkin-Elmer spectrophotometer; samples were run as KBr pellets. ^{1}H NMR spectra were recorded at 250.13 MHz using a Bruker WM250 spectrometer. Chemical shifts are given in parts per million (ppm) versus $SiMe_4$ and deuterated dimethylsulfoxide as solvent. Solid state CD spectra were recorded with a JASCO J-720 spectropolarimeter using KBr disks. Magnetic data were obtained with a Quantum Design MPMS SQUID susceptometer. All samples were 3 mm diameter pellets molded from ground crystalline samples. Magnetic susceptibility measurements were performed in the 2−300 K temperature range under a 0.1 T applied magnetic field, and diamagnetic corrections were applied by using Pascal's constants.[18] Isothermal magnetization measurements were performed up to 5 T at 2 K. The magnetic susceptibilities have been computed by exact calculations of the energy levels associated to the spin Hamiltonian through diagonalization of the full matrix with a general program for axial symmetry,[19] and with the MAGPACK program package[20] in the case of magnetization. Least-squares fittings were accomplished with an adapted version of the function-minimization program MINUIT.[21] Mössbauer measurements were carried out on a constant-acceleration conventional spectrometer with a 50 mCi source of ^{57}Co (Rh matrix). Isomer shift values (δ) throughout the paper are given with respect to metallic iron at room temperature. The absorber was a sample of 80 mg of microcrystalline powder enclosed in a 20 mm diameter cylindrical plastic sample-holder, the size of which had been determined to optimize the absorption. Variable-temperature spectra were obtained in the 4.5−300 K range, by using a MD 306 Oxford cryostat, the thermal scanning being monitored by an Oxford ITC4 servocontrol device (±0.1 K accuracy). A least-squares computer program[22] was used to fit the Mössbauer parameters and determine their standard deviations of statistical origin (given in parentheses).

Crystallographic Data Collection and Structure Determination for the Complexes 1, 2, 3, 5, 6, 7, 8, 9, and 10. Crystals of **1**, **2**, **3**, **5**, **6**, **7**, **8**, **9**, and **10** were kept in the mother liquor until they were dipped into oil. The chosen crystals were mounted on a Mitegen micromount and quickly cooled down to 180 or 150 K. The selected crystals of **1** (orange, 0.2 × 0.15 × 0.08 mm^3), **2** (orange, 0.25 × 0.07 × 0.05 mm^3), **3** (orange, 0.375 × 0.15 × 0.125 mm^3), **5** (yellow green, 0.5 × 0.375 × 0.125 mm^3), **6** (yellow, 0.35 × 0.2 × 0.12 mm^3), **7** (yellow green, 0.35 × 0.25 × 0.2 mm^3), **8** (red, 0.3 × 0.25 × 0.2 mm^3), **9** (red, 0.12 × 0.12 × 0.1 mm^3), **10** (red, 0.35 × 0.2 × 0.17 mm^3) were mounted on a Stoe Imaging Plate Diffractometer System (IPDS) (**1**, **6**, **8**, **9**) or an Oxford-Diffraction XCALIBUR (**3**, **5**, **7**, **10**) using a graphite monochromator (λ = 0.71073 Å) and equipped with an Oxford Cryosystems cooler device. The data were collected at 180 (**1**, **2**, **3**, **5**, **7**, **10**) or 150 K (**6**, **8**, **9**). The unit cell determination and data integration were carried out using the CrysAlis RED package for the data recorded on the Xcalibur and the Xred package for the STOE.[23,24] A total of 95813 reflections were collected for **1**, of which 19118 were independent (R_{int} = 0.1733), 87201 reflections for **2**, of which 23148 were independent (R_{int} = 0.0438), 44289 reflections for **3**, of which 11485 were independent (R_{int} = 0.0583), 46726 reflections for **5**, of which 12511 were independent (R_{int} = 0.0481), 48777 reflections for **6**, of which 11964 were independent (R_{int} = 0.0609), 46828 reflections for **7**, of which 12461 were independent (R_{int} = 0.0488), 60249 reflections for **8**, of which 11856 were independent (R_{int} = 0.0729), 60152 reflections for **9**, of which 11767 were independent (R_{int} = 0.0848), and 43978 reflections for **10**, of which 11349 were independent (R_{int} = 0.0488). The structures have been solved by Direct Methods using SIR92,[25] and refined by least-squares procedures on F^2 with the program SHELXL97[26] included in the softwares package WinGX version 1.63.[27] Atomic Scattering Factors were taken from the International tables for X-ray Crystallography.[28] All hydrogen atoms were geometrically placed and refined by using a riding model. All non-hydrogen atoms were anisotropically refined, and in the last cycles of refinement a weighting scheme was used, where weights are calculated from the following formula: $w = 1/[\sigma^2(F_o^2) + (aP)^2 + bP]$ where $P = (F_o^2 + 2F_c^2)/3$. Drawings of molecules are performed with the program ORTEP32[29] with 30% probability displacement ellipsoids for non-hydrogen atoms. It was not possible to resolve diffuse electron-density residuals (one CH_3OH molecule) for complexes **5** and **6**. Treatment with the SQUEEZE facility from PLATON[30] resulted in a smooth refinement. Since a few low order reflections are missing from the data set, the electron count is underestimated. Thus, the values given for *D*(calc), *F*(000), and the molecular weight are only valid for the ordered part of the structure.

Results

The first reactions were carried out with a 1:1 3d/4f ratio, in the hope of obtaining heterodinuclear 3d−4f complexes, while a 2:1 3d/4f ratio was used for the following ones. Both types of reaction conditions yielded the same 2:1 3d/4f complexes. Once isolated and dried, the crystals of complexes **1**−**13** are stable in the open atmosphere. The analytical results do confirm the trinuclear character of the isolated complexes. In all cases, the lanthanide ions were introduced as nitrate salts while perchlorate salts were used for iron(II) and acetates for cobalt(II), manganese(II), and zinc(II). The trinuclear complexes were isolated as cationic entities with perchlorate (**8**−**11**, Fe−Ln) or nitrate (**1**−**7**, **12**, **13**, other 3d−Ln) as the counteranion. The presence of ligand is evidenced by several intense bands in the IR spectra. The bands around 1620 cm^{-1} correspond to the stretching vibrations of the C=N (imine) bonds while the sharp bands

(18) Pascal, P. *Ann. Chim. Phys.* **1910**, *19*, 5–70.
(19) Boudalis, A. K.; Clemente-Juan, J.-M.; Dahan, F.; Tuchagues, J.-P. *Inorg. Chem.* **2004**, *43*, 1574–1586.
(20) (a) Borrás-Almenar, J. J.; Clemente-Juan, J. M.; Coronado, E.; Tsukerblat, B. S. *Inorg. Chem.* **1999**, *38*, 6081–6088. (b) Borrás-Almenar, J. J.; Clemente-Juan, J. M.; Coronado, E.; Tsukerblat, B. S. *J. Comput. Chem.* **2001**, *22*, 985–991.
(21) James, F.; Roos, M. *MINUIT Program*, a System for Function Minimization and Analysis of the Parameters Errors and Correlations. *Comput. Phys. Commun.*, **1975**, *10*, 343−367.
(22) Lagarrec, K. *Recoil, Mössbauer Analysis Software for windows*; http://www.physics.uottawa.ca/~recoil
(23) *CrysAlis RED*, version 1.170.32; Oxford Diffraction Ltd.: Abingdon, U.K., 2003.
(24) *STOE: IPDS Manual*, version 2.75; Stoe & Cie: Darmstadt, Germany, 1996.
(25) *SIR92* - A program for crystal structure solution. Altomare, A.; Cascarano, G.; Giacovazzo, C.; Guagliardi, A. *J. Appl. Crystallogr.* **1993**, *26*, 343–350.
(26) Sheldrick, G. M. *SHELX97* [*Includes SHELXS97, SHELXL97, CIFTAB*] - *Programs for Crystal Structure Analysis*, Release 97-2; Institüt für Anorganische Chemie, Universität Göttingen: Göttingen, Germany, 1998.
(27) *WINGX* - 1.63 Integrated System of Windows Programs for the Solution, Refinement and Analysis of Single Crystal X-Ray Diffraction Data. Farrugia, L. *J. Appl. Crystallogr.* **1999**, *32*, 837–840.
(28) *International tables for X-ray crystallography*; Kynoch press: Birmingham, England, 1974; Vol *IV*.
(29) *ORTEP3 for Windows*; Farrugia, L. J. *J. Appl. Crystallogr.* **1997**, *30*, 565.
(30) Sluis, P. v.d.; Spek, A. L. *Acta Crystallogr.* **1990**, *A46*, 194–201.

Table 1. Crystallographic Data for Complexes [LCoGdCoL]NO_3, **1**, [LCoTbCoL]NO_3, **2**, [LCoDyCoL]$NO_3 \cdot CH_3OH$, **3**, [LMnGdMnL]NO_3, **5**, [LMnTbMnL]NO_3, **6**, [LMnDyMnL]$NO_3 \cdot CH_3OH$, **7**, [LFeGdFeL]ClO_4, **8**, [LFeTbFeL]$ClO_4 \cdot CH_3OH$, **9**, and [LFeDyFeL]$ClO_4 \cdot CH_3OH$, **10**

	1	**2**	**3**	**5**	**6**
formula	$C_{58}H_{60}Co_2GdN_7O_{15}$	$C_{58}H_{60}Co_2N_7O_{15}Tb$	$C_{59}H_{64}Co_2DyN_7O_{16}$	$C_{58}H_{60}GdMn_2N_7O_{15}$	$C_{58}H_{60}Mn_2GdN_7O_{15}$
Fw	1370.24	1371.92	1407.53	1362.26	1363.93
space group	$C2/c$	$C2/c$	$P2_12_12_1$	$P2_12_12_1$	$P2_12_12_1$
a, Å	47.246(9)	47.7980(14)	15.7227(10)	15.6720(7)	15.6736(10)
b, Å	24.634(5)	24.7480(8)	15.8241(10)	15.9438(7)	24.5055(19)
c, Å	17.997(4)	17.9420(5)	24.3813(15)	24.5234(11)	15.9210(11)
α, deg	90	90	90	90	90
β, deg	111.02(3)	111.386(1)	90	90	90
γ, deg	90	90	90	90	90
V, Å^{-3}	19552(8)	19762(1)	6066.0(7)	6127.7(5)	6115.1(7)
Z	12	12	4	4	4
ρ_{calcd}, g cm^{-3}	1.396	1.383	1.541	1.477	1.481
λ, Å	0.71073	0.71073	0.71073	0.71073	0.71073
T, K	180(2)	180(2)	180(2)	180(2)	150(2)
μ (Mo Kα), mm^{-1}	1.574	1.624	1.833	1.545	1.62
R^a obs, all	0.0497, 0.1727	0.0457, 0.0774	0.0384, 0.0485	0.0363, 0.0411	0.0444, 0.0509
Rw^b obs, all	0.0942, 0.1185	0.1188, 0.1282	0.0914, 0.0945	0.0968, 0.0997	0.1084, 0.1142

	7	**8**	**9**	**10**
formula	$C_{59}H_{64}DyMn_2N_7O_{16}$	$C_{58}H_{60}ClFe_2GdN_6O_{16}$	$C_{59}H_{64}ClFe_2N_6O_{17}Tb$	$C_{59}H_{64}ClDyFe_2N_6O_{17}$
Fw	1399.55	1401.52	1435.23	1438.81
space group	$P2_12_12_1$	$P2_12_12_1$	$P2_12_12_1$	$P2_12_12_1$
a, Å	15.6534(7)	15.779(3)	15.6954(12)	15.6543(7)
b, Å	15.9509(8)	15.973(3)	24.0336(19)	15.9364(8)
c, Å	24.4890(13)	24.064(5)	15.9343(12)	24.0870(11)
α, deg	90	90	90	90
β, deg	90	90	90	90
γ, deg	90	90	90	90
V, Å^{-3}	6114.6(5)	6065(2)	6010.7(8)	6009.1(5)
Z	4	4	4	4
ρ_{calcd}, g cm^{-3}	1.52	1.535	1.586	1.59
λ, Å	0.71073	0.71073	0.71073	0.71073
T, K	180(2)	150(2)	150(2)	180(2)
μ (Mo Kα), mm^{-1}	1.689	1.668	1.76	1.827
R^a obs, all	0.0358, 0.0391	0.0384, 0.0485	0.05, 0.0763	0.0401, 0.0518
Rw^b obs, all	0.0931, 0.0957	0.0914, 0.0945	0.1143, 0.1278	0.1099, 0.1163

$^a R = \sum||F_o| - |F_c||/\sum|F_o|$. $^b wR_2 = [\sum w(F_o^2 - F_c^2)^2/\sum w(F_o^2)^2]^{1/2}$.

at 1384 cm^{-1} and the broad bands at 1080 cm^{-1} can be assigned to ionic nitrate or perchlorate anions.[31]

Description of the Structures. Complexes [LMnLnMnL]NO_3, **5**−**7**, and [LFeLnFeL]ClO_4, **8**−**10**, with Ln = Gd, Tb, Dy crystallize in the chiral space group $P2_12_12_1$ with $Z = 4$. The situation is more complex for the [LCoLnCoL]NO_3 series, where the [LCoDyCoL]$NO_3 \cdot CH_3OH$ complex **3** is the only one crystallizing in the $P2_12_12_1$ space group. The other [LCoLnCoL]NO_3 complexes (Ln = Gd, **1**, Tb, **2**) crystallize in the centrosymmetric $C2/c$ space group with $Z = 12$. The crystallographic data of the different complexes are collated in Table 1, and selected bond lengths and angles are collated in Supporting Information, Tables S1−S3. These complexes being distributed among two series of isomorphous crystalline species, **1**, **2** and **3**, **5**−**10**, we describe the structure of one complex in each series. The crystal structures of complexes **5**, **6**, and **8** consist of one $[LMnGdMnL]^+$, $[LMnTbMnL]^+$, and $[LFeGdFeL]^+$ cationic entity along with either a nitrate or a perchlorate anion while a supplementary methanol molecule is involved in the asymmetric units of complexes [LCoDyCoL]$NO_3 \cdot CH_3OH$ **3**, [LMnDyMnL]$NO_3 \cdot CH_3OH$ **7**, [LFeTbFeL]$ClO_4 \cdot CH_3OH$ **9**, and [LFeDyFeL]$ClO_4 \cdot CH_3OH$ **10**. Views of the cationic $[LMnGdMnL]^+$ and $[LFeGdFeL]^+$ cores of **5** and **8** are shown in Figures 1 and 2, respectively. Each Mn^{II} ion is coordinated to the inner N_3O_3 coordination site of the trideprotonated L^{3-} ligand. In **5**, two $[MnL]^-$ building units are assembled by the gadolinium ion through the three phenoxo oxygen atoms of each $[MnL]^-$ unit to form a face-sharing trinuclear molecule. These phenoxo oxygen atoms bridge the metal ions to yield a practically linear MnGdMn core, with a Mn···Gd···Mn angle of 178.88(2)° and equivalent Mn···Gd distances (3.3355(7), 3.3339(7) Å). While the Mn−N bonds are almost the same for the two Mn ions (2.184(4)−2.204(4) Å), this is not true for the Mn−O bonds, where one bond (2.165(3), 2.172(3) Å) is longer than the other two (2.128(3)−2.146(3) Å). The screw arrangement of the achiral tripodal ligand around the 3d ion yields chiral Λ or Δ configurations, and the assembly of two chiral molecules by the Ln ion may yield either homochiral (Λ−Λ or Δ−Δ) or heterochiral (Λ−Δ) pairs. The present complex crystallizes in a non-centrosymmetric space group $P2_12_12_1$: complex **5** is thus a conglomerate, and the structurally determined crystal corresponds to the homochiral Λ−Λ pair shown in Figure 1. Unfortunately, it is very difficult to separate the Δ−Δ and Λ−Λ crystals from the conglomerate for the probability to find hemihedral faces in the $P2_12_12_1$ space group is poor.[32] The Gd ion may be considered as 12 coordinate, with two very different ranges of Gd−O bond lengths. Indeed, there are

(31) Nakamoto, K. *Infrared and Raman Spectra of Inorganic and Coordination Compounds*, 5th ed.; Wiley: New York, 1997.

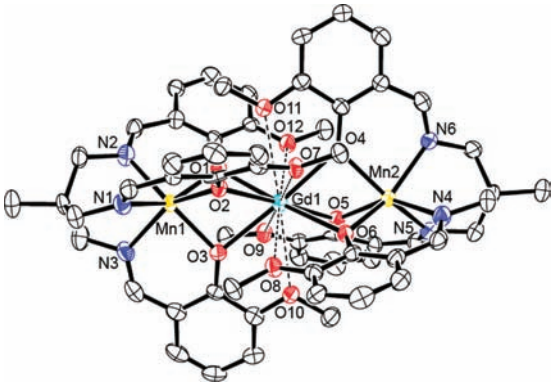

Figure 1. Molecular structure of the trinuclear $[LMnGdMnL]^+$ entity **5**, with the thermal ellipsoids drawn at the 30% probability level. Hydrogen atoms are omitted for clarity. Selected bond lengths, distances (Å) and angles (deg): Mn(1)−N_{avg} 2.191(4), Mn(1)−O(1) 2.172(3), Mn(1)−O(2) 2.138(3), Mn(1)−O(3) 2.128(3), Mn(2)−N_{avg} 2.195(4), Mn(2)−O(4) 2.165(3), Mn(2)−O(5) 2.146(3), Mn(2)−O(6) 2.143(3), Gd−$O_{phen(avg)}$ 2.413(3), Gd−$O_{OMe(avg)}$ 2.924(3), Mn(1)···Gd 3.3339(7), Mn(2)···Gd 3.3355(7), Mn(1)−Gd−Mn(2) 177.88(2).

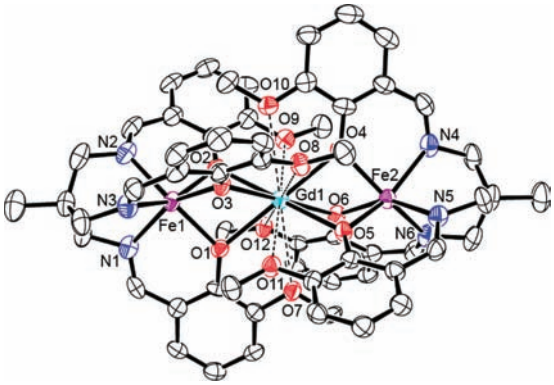

Figure 2. Molecular structure of the $[LFeGdFeL]^+$ entity **8**, with the thermal ellipsoids drawn at the 30% probability level. Hydrogen atoms are omitted for clarity. Selected bond lengths, distances (Å) and angles (deg): Fe(1)−N_{avg} 2.151(4), Fe(1)−O(1) 2.102(3), Fe(1)−O(2) 2.092(3), Fe(1)−O(3) 2.112(3), Fe(2)−N_{avg} 2.151(4), Fe(2)−O(4) 2.110(3), Fe(2)−O(5) 2.114(3), Fe(2)−O(6) 2.100(3), Gd−$O_{phen(avg)}$ 2.391(3), Gd−$O_{OMe(avg)}$ 2.917(4), Fe(1)···Gd 3.2960(9), Fe(2)···Gd 3.2905(9), Fe(1)−Gd−Fe(2) 178.19(2).

only two different types of oxygen atoms linked to the Gd ion, the deprotonated phenoxo oxygens with bond lengths varying from 2.400(3) to 2.434(3) Å and the neutral methoxy oxygens characterized by larger bond lengths, from 2.885(3) to 2.971(3) Å. Although the latter bonds are long, they prevent the Gd ion from interacting with other possible ligands or anions, such as the nitrate anions present here as simple counterions.

Furthermore, the presence of methoxy groups in the ortho-position of the phenol functions promotes linking of the lanthanide cation between the two $[MnL]^-$ building units. In view of the tripodal nature of the ligands, an ideal overlapping implies a 60° rotation of a $[MnL]^-$ unit with respect to the other one. In the present case, the angle

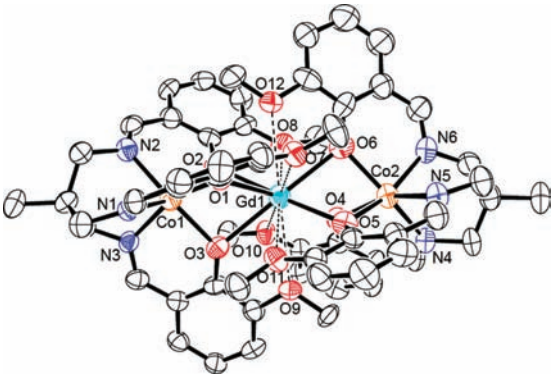

Figure 3. Molecular structure of the non-symmetrical trinuclear $[LCoGdCoL]^+$ entity **1**, with the thermal ellipsoids drawn at the 30% probability level. Hydrogen atoms are omitted for clarity. Selected bond lengths, distances (Å), and angles (deg): Co(1)−N_{avg} 2.106(6), Co(1)−O(1) 2.080(5), Co(1)−O(2) 2.085(5), Co(1)−O(3) 2.076(5), Co(2)−N_{avg} 2.090(7), Co(2)−O(4) 2.076(5), Co(2)−O(5) 2.077(5), Co(2)−O(6) 2.057(5), Gd−$O_{phen(avg)}$ 2.418(5), Gd−$O_{OMe(avg)}$ 2.919(5), Co(1)···Gd 3.321(1), Co(2)···Gd 3.313(1), Co(1)−Gd−Co(2) 178.41(5).

is 54−55°, or 65−66°, depending on the reference, thus deviating by about 5° from the ideal case. The Fe^{II} complexes **8**−**10**, with perchlorate as counterions, crystallize in the non-centrosymmetric space group $P2_12_12_1$, as specified previously.

The complexes $[LCoGdCoL]NO_3$ **1** and $[LCoTbCoL]NO_3$, **2**, crystallize in the $C2/c$ centrosymmetric space group with $Z = 12$. Both Λ−Λ and Δ−Δ pairs coexist in these racemic crystals, and heterochiral (Λ−Δ) pairs are again absent. In comparison with the complexes described above, the main difference arises from the fact that the asymmetric unit contains two different [LCoGdCoL] entities. The first one is similar to the one observed in the chiral space group (Figure 3), with two slightly different cobalt environments, while in the second one the LCo building units are symmetry related through the Gd ion, which results in the presence of 12 molecules by unit cell ($Z = 12$). The symmetrical [LCoGdCoL] entity is characterized by slightly shorter Co−O bonds, av. 2.059 Å instead of av. 2.070 and 2.080 Å in the dissymmetrical one. These two [LCoGdCoL] entities still correspond to linear trinuclear complex molecules, with similar Co···Gd···Co angles (178.41(5)° and 178.68(5)°), and slightly different Co···Gd distances (3.331(1) Å for the symmetrical unit against 3.313(1) and 3.321(1) Å for the dissymmetrical one). There is significant difference in the Gd−O bond lengths, with again six short and six larger bonds. ORTEP views of the other complexes are displayed in the Supporting Information, Figures S1−S6 for complexes **2**, **3**, **6**, **7**, **9**, **10**, respectively.

The coordination geometry around each Mn, Co, or Fe metal ion is intermediate between a regular octahedron and a trigonal prism. This deformation is easily analyzed with the help of the "SHAPE" program.[33] For species crystallizing in a chiral space group, the trigonal prism is preferred to the octahedron, and the 3d environments are best described as distorted trigonal prisms, with distortions increasing in the order **5** = **6** = **7** < **8** = **9** = **10** < **3** (Supporting Information, Table S4). The analysis is less

(32) (a) Bosnich, B.; Phillip, A. T. *J. Am. Chem. Soc.* **1968**, *90*, 6352–6359. (b) Hidaka, J.; Douglas, B. E. *Inorg. Chem.* **1964**, *3*, 1180–1184. (c) Canary, J. W.; Allen, C. S. *J. Am. Chem. Soc.* **1995**, *117*, 8484–8485. (d) Zahn, S.; Canary, J. W. *Angew. Chem., Int. Ed.* **1998**, *37*, 305–307. (e) Castagnetto, J. M.; Canary, J. W. *Chem. Commun.* **1998**, 203–204.

(33) Alvarez, S.; Avnir, D.; Llunell, M.; Pinsky, M. *New J. Chem.* **2002**, *26*, 996–1009.

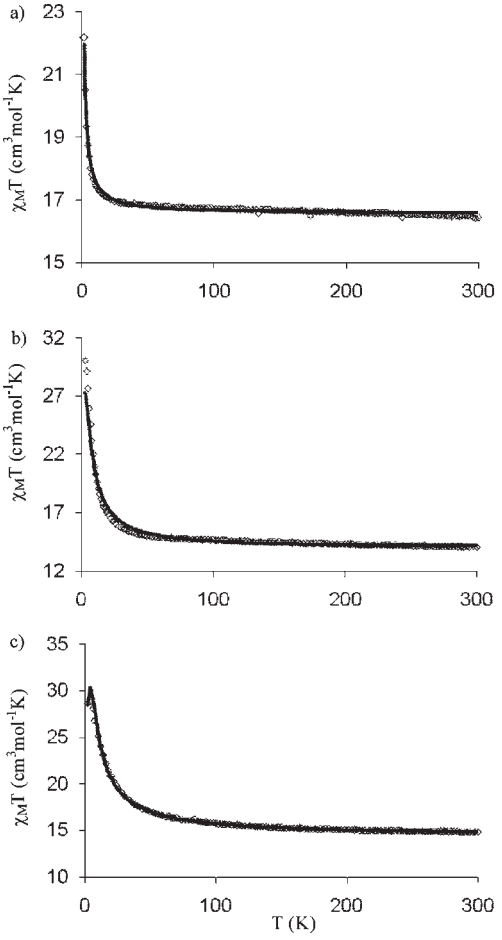

Figure 4. Temperature dependence of the $\chi_M T$ products for (a) [LMnGdMnL]NO_3 **5**, (b) [LCoGdCoL]NO_3 **1**, and (c) [LFeGdFeL]ClO_4 **8**.

straightforward for the species crystallizing in the $C2/c$ space group. The cobalt environment in the non-symmetrical [LCoGdCoL] units of **1** can be considered as a distorted trigonal prism while the cobalt environment is best described as a distorted octahedron in the symmetrical [LCoGdCoL] units. It is worth noting that distortion of the trigonal prism is larger in complex **1** than in **3** (Supporting Information, Table S4). These distortions correspond to the Bailar trigonal twist for the Bailar-twist symmetry constant found for the entire set of the present series of complexes (4.3) does not differ from the value expected for a pure Bailar-twist route (4.2).[34] Whatever the space group is, there are no hydrogen bonds between adjacent trinuclear complexes, and the shorter 3d···3d intermolecular distances are around or larger than 8 Å, resulting in trinuclear complexes well isolated from each other.

Magnetic Properties. The magnetic susceptibilities of the [LCoLnCoL]NO_3, [LMnLnMnL]NO_3, and [LFeLnFeL]-ClO_4 complexes **1**−**10** (Ln = La, Gd, Tb, Dy) have been measured in the 2−300 K temperature range under an applied magnetic field of 0.1 T. The simpler example being the [LMnGdMnL]NO_3 complex **5**, which may be analyzed by using a simple isotropic spin Hamiltonian; it will be examined first. The thermal variation of the $\chi_M T$ product for complex **5** is displayed in Figure 4a, χ_M being the molar magnetic susceptibility of the trinuclear species corrected for the diamagnetism of the ligands. At 300 K, $\chi_M T$ is equal to 16.44 cm^3 mol^{-1} K which corresponds to the value expected for uncoupled manganese (two) and gadolinium (one) ions (16.62 cm^3 mol^{-1} K). Lowering the temperature results in a slow increase of $\chi_M T$ down to 20 K (17.1 cm^3 mol^{-1} K) and then in a more abrupt one, up to 22.2 cm^3 mol^{-1} K at 2 K. This behavior indicates that a ferromagnetic interaction between the Mn^{II} ($S = 5/2$) and Gd^{III} ($S = 7/2$) ions operates at low temperature. A quantitative analysis has been performed on the basis of an expression derived from the spin-only Hamiltonian for the spin system Mn1−Gd−Mn2,

$$H = -J_{Mn_1Gd}S_{Mn_1}S_{Gd} - J_{Mn_2Gd}S_{Mn_2}S_{Gd} - j_{Mn_1Mn_2}S_{Mn_1}S_{Mn_2}$$

The magnetic susceptibility has been computed by exact calculation of the energy levels associated with the spin Hamiltonian through diagonalization of the full E-matrix. The magnetic data have been correctly fitted with a unique J value ($J_{Mn1Gd} = J_{Mn2Gd}$) and an interaction parameter j_{Mn1Mn2} equal to zero. The best fit yielded a J value of 0.08 cm^{-1} with $g = 2.0$ and a nice agreement factor $R = \sum[(\chi_M T)_{obs} - (\chi_M T)_{calc}]^2/\sum[(\chi_M T)_{obs}]^2$ equal to 3×10^{-5}.

Because of the orbital degeneracy of high-spin cobalt(II) ($S = 3/2$), interpretation of the data by using an isotropic spin Hamiltonian is not rigorous for the [LCoGdCoL]NO_3 complex **1**. Indeed, the exchange phenomenon in the presence of orbital degeneracy is an open problem for which no general solution is available. Furthermore, the Kotani expressions,[35] appropriate with isolated cobalt(II) centers, are not suitable here because of the Co−Gd magnetic interaction. It has been previously shown that the orbital contribution is significantly quenched when the iron(II) or cobalt(II) environment deviates from ideal octahedral geometry.[36,6] This is the case for complexes **1** and **8** where the cobalt(II) and iron(II) centers are hexacoordinate with a strong deformation from octahedron (see Discussion); in such a case, the orbital degeneracy can only weakly affect the temperature dependence of the $\chi_M T$ product.[37,38] The data obtained for complex **1** are displayed in Figure 4b. At 300 K, the $\chi_M T$ product is equal to 14.4 cm^3 mol^{-1} K. Upon lowering the temperature, $\chi_M T$ gradually increases to 30.7 cm^3 mol^{-1} K at 7 K, indicating the presence of a ferromagnetic interaction. Surprisingly, attempts to fit the data by using the simplified $H = -2JS_{Co}S_{Gd}$ Hamiltonian yields satisfactory results, indicating that zero field splitting (ZFS) of cobalt(II) can be neglected. The best fit for complex **1**, [LCoGdCoL]NO_3, was obtained for the following set of parameters, $J = 0.52$ cm^{-1}, $g = 2.21$. The energy levels and magnetic properties of spin systems including the anisotropic cobalt(II) ion usually require consideration of single ion ZFS terms. This ZFS term includes the anisotropy originating from the orbital contribution. The simpler spin Hamiltonian that may be used is $H = -2JS_{Co}S_{Gd} + 2D_{Co}S_z{}^2{}_{Co} + \Sigma_{i,j}$

(34) Bailar, J. C., Jr. *J. Inorg. Nucl. Chem.* **1958**, *8*, 165–175.
(35) Kotani, M. *J. Phys. Soc. Jpn.* **1949**, *4*, 293.
(36) Borras-Almenar, J. J.; Clemente-Juan, J. M.; Coronado, E.; Palii, A. V.; Tsukerblat, B. S. *J. Phys. Chem. A* **1998**, *102*, 200–213.
(37) Carlin, R. L. *Magnetochemistry*; Springer-Verlag: New York, 1986.
(38) *Theory and Applications of Molecular Magnetism*; Boudreaux, E. A., Mulay, L. N., Eds.; Wiley-Interscience: New York, 1976.

$g_i\beta H_j S_{ij}$ in which the first term gauged by the parameter J accounts for the spin exchange interaction, the second one gauged by D accounts for axial single ion ZFS of cobalt(II), and the third one accounts for the Zeeman contributions where i = Co, Gd and $j = x, y, z$. The temperature dependence of $\chi_M T$ was fitted using the above Hamiltonian. The best fit for complex **1**(Figure 4b) was obtained for the following set of parameters, $J = 0.52\ cm^{-1}$, $D = 0.1\ cm^{-1}$, $g = 2.21$.[20]

These results are in complete agreement with the data originating from the magnetic study of the [LCoLaCoL]$NO_3 \cdot CH_3OH$ complex, **4**, in which the two cobalt ions are isolated by a diamagnetic lanthanum ion. The $\chi_M T$ value, equal to 5.72 $cm^3\ mol^{-1}$ K at room temperature (Supporting Information, Figure S7), is practically constant down to 100 K, then it decreases slowly from 100 to 5 K (4.8 $cm^3\ mol^{-1}$ K) and slightly more abruptly from 5 to 2 K (4.4 $cm^3\ mol^{-1}$ K). The $\chi_M T$ value at room temperature allows an estimation of the g_{Co} parameter, which is found to be 2.44. From this value and a g_{Gd} value of 2.0, the g parameter for the $S = 13/2$ ground state corresponding to a ferromagnetic Co−Gd interaction is estimated to 2.20, in perfect agreement with that resulting from the fit ($g = 2.21$).[39] Furthermore, the weak $\chi_M T$ decrease observed at low temperature for complex **4** confirms the low value of the ZFS term and the absence of Co−Co interaction through the diamagnetic La ion.

Complex **8**, [LFeGdFeL]ClO_4, behaves as the equivalent cobalt complex **1**. Figure 4c shows the temperature dependence of the $\chi_M T$ product for **8**. After a smooth increase from 300 (14.79 $cm^3\ mol^{-1}$ K) to 70 K (16.30 $cm^3\ mol^{-1}$ K), $\chi_M T$ increases more sharply, up to 28.86 $cm^3\ mol^{-1}$ K at 4 K before decreasing to 28.64 $cm^3\ mol^{-1}$ K at 2 K. The best fit obtained with the Hamiltonian described hereafter yields the following set of parameters: $J = 0.69\ cm^{-1}$, $D = 5.7\ cm^{-1}$, $g = 2.04$, with an agreement factor equal to 5×10^{-5}. These parameters allow a nice fit of the field dependence of magnetization for **8** (Supporting Information, Figure S17). The large ZFS of the Fe ions is quite well evidenced by the $\chi_M T$ variation and the field dependence of magnetization for the complex [LFeLaFeL]$ClO_4 \cdot CH_3OH$ **11** (Supporting Information, Figure S8), which can be satisfactorily fitted by considering solely an axial ZFS term ($D = 7\ cm^{-1}$). It is worth noting that the D parameters found for complexes **8** and **11** are very similar (5.7 and 7 cm^{-1}).

Orbital contributions originating from the lanthanide ions operate in the trinuclear cobalt (**2**, **3**), manganese (**6**, **7**), and iron (**9**, **10**) complexes involving Tb and Dy ions. Furthermore, the cobalt(II) and iron(II) cations are also characterized by non-negligible orbital contributions. In these six complexes, it is thus only possible to qualitatively estimate the isotropic magnetic interaction, for operation of first-order angular momenta prevents from relying on spin-only Hamiltonians to quantitatively interpret the experimental magnetic susceptibility data. Indeed, two magnetic phenomena, strong spin−orbit coupling and M−Ln isotropic magnetic interactions, are present. The strong spin−orbit coupling is responsible for the $\chi_M T$ decrease observed in the temperature dependence of the $\chi_M T$ product of complexes **12**, [LZnTbZnL]$NO_3 \cdot 3H_2O$, and **13**, [LZnDyZnL]$NO_3 \cdot 2H_2O$, where the Ln ions are the only ones to be magnetically active. The $\chi_M T$ product for **13**, equal to 14 $cm^3\ mol^{-1}$ K and constant down to 100 K (13.8 $cm^3\ mol^{-1}$ K), decreases to 9.66 $cm^3\ mol^{-1}$ K at 2 K (Supporting Information, Figure S9). For complex **12** the $\chi_M T$ value is lower at 300 K (12.0 $cm^3\ mol^{-1}$ K) and the decrease, which begins at higher temperature (180 K), is less important (10.2 $cm^3\ mol^{-1}$ K at 2 K) (Supporting Information, Figure S10). The $\chi_M T$ values at 300 K correspond perfectly to those expected for isolated Dy (14.17 $cm^3\ mol^{-1}$ K) and Tb (11.82 $cm^3\ mol^{-1}$ K) ions, respectively. A look at the $\chi_M T$ versus T variations for the [LCoDyCoL]$NO_3 \cdot CH_3OH$ (**3**) and [LMnDyMnL]$NO_3 \cdot CH_3OH$ (**7**) complexes indicates that the $\chi_M T$ values slightly increase from 300 to 80 K (from 21.0 to 21.8 $cm^3\ mol^{-1}$ K and from 23.3 to 23.6 $cm^3\ mol^{-1}$ K, respectively), then go through a minimum (21.6 and 23.3 $cm^3\ mol^{-1}$ K, respectively) before increasing sharply to 31.9 and 28.8 $cm^3\ mol^{-1}$ K, respectively (Supporting Information, Figures S11, S12). The room temperature values do correspond to those expected for non interacting Co^{II} (2) and Dy^{III} (1) cations (**3**), and Mn^{II} (2) and Dy^{III} (1) cations (**7**). Observation of a minimum in these $\chi_M T$ versus T variations indicates operation of two antagonistic effects, the spin−orbit coupling which is responsible for the slight $\chi_M T$ decrease, and the ferromagnetic M−Ln interactions which result in an increase of the $\chi_M T$ product at low temperature. The equivalent Tb complexes, [LCoTbCoL]NO_3, **2**, and [LMnTbMnL]NO_3, **6**, behave similarly (Supporting Information, Figures S13 and S14), except that minima are not visible in their $\chi_M T$ versus T variations. These results confirm the presence of ferromagnetic interactions in complexes **2**, **3**, **6**, and **7** and suggest that the Co−Tb and Mn−Tb interactions are slightly larger than the corresponding Co−Dy and Mn−Dy ones (Supporting Information, Figures S11, S12). Furthermore, these similarities in the Mn and Co complexes again do agree with operation of weaker ZFS terms for cobalt. At variance, the $\chi_M T$ versus T variations for the equivalent iron complexes **9** and **10** evidence operation of larger ZFS terms. Nevertheless, ferromagnetic Fe−Tb and Fe−Dy interactions also operate (Supporting Information, Figures S15, S16).

To find out whether our compounds show SMM behavior, we performed alternating current (ac) susceptibility measurements in the 2−10 K range using a MPMS SQUID magnetometer with a zero direct current (dc) field and a 3 Oe ac field oscillating at 10−1000 Hz. Below 5 K, a frequency-dependent decrease in the in-phase (χ'_M) susceptibility signal along with a concomitant increase of the out of phase (χ''_M) susceptibility signal were observed for the cobalt complexes **1**, **2**, and **3**. At variance, manganese (**6**, **7**) and iron (**8**, **9**, **10**) complexes did not exhibit χ''_M values different from zero in the 2−10 K temperature range. Consequently, we performed magnetization hysteresis loop and magnetization relaxation measurements using a micro-SQUID apparatus[40] mainly on the more interesting cobalt samples, to study the magnetization dynamics down to 0.04 K and to confirm their SMM properties.

(39) Scaringe, R. P.; Hodgson, D. J.; Hatfield, W. E. *Mol. Phys.* **1978**, *35*, 701–713.

(40) Bonet Orozco, E.; Wernsdorfer, W.; Barbara, B.; Benoit, A.; Mailly, D.; Thiaville, A. *Phys. Rev. Lett.* **1999**, *83*, 4188–4191.

The studies were performed on single microcrystals, which were thermalized using Apiezon grease. The field was aligned with the easy axes of magnetization using the transverse field method.[41] Figure 5a and Supporting Information, Figure S18 show magnetization versus magnetic field hysteresis loops for a single crystal of **1** at different temperatures and field sweep rates. Large hysteresis loops, observed below 1.1 K whose coercivity is temperature and sweep-rate dependent, increasing with decreasing temperature and increasing field sweep rate, do agree with a slow relaxation of magnetization and confirm the superparamagnetic-like behavior of complex **1**, $[LCoGdCoL]NO_3$, as expected for an SMM below its blocking temperature. Very similar magnetization hysteresis loops were observed for complexes **2**, $[LCoTbCo]NO_3$, (Figure 5b, Supporting Information, Figures S19 and S20) and **3**, $[LCoDyCoL]NO_3 \cdot CH_3OH$, (Figure 5c, Supporting Information, Figures S21 and S22), the later complex being characterized by narrower loops. A very different behavior was observed for complex **6**, $[LMnTbMnL]NO_3$, whose hysteresis loops appear below 0.2 K with a coercive field of 240 Oe (Supporting Information, Figure S23), at variance with the 8860 and 7330 Oe values obtained for complexes **1** and **2**, respectively. Complex **9**, $[LFeTbFeL]ClO_4 \cdot CH_3OH$, which exhibits a very narrow hysteresis loop at 0.04 K exclusively (Supporting Information, Figure S24) is almost devoid of SMM behavior, while complexes **4**, $[LCoLaCoL]NO_3 \cdot CH_3OH$, **12**, $[LZnTbZnL]NO_3 \cdot 3H_2O$, and **13**, $[LZnDyZnL]NO_3 \cdot 2H_2O$, do not exhibit any hysteresis loop, even at 0.04 K.

The slow relaxation of magnetization previously observed in the M versus H plots has been studied through ac field susceptibility measurements from 1.8 to 8 K. At zero dc field, frequency-dependent out of phase ac signals, χ'', appear for complexes **1**, **2**, and **3** when the applied frequencies vary from 1 to 1500 Hz (Supporting Information, Figure S25 for complex **1**). Fits of the thermally activated region to the Arrhenius relationship of equation $\tau = \tau_0 \exp(\Delta_{eff}/T)$, with τ defining the relaxation time and τ_0 the pre-exponential factor yielded $U_{eff} = 21.3$ K, 14.5 K and $\tau_0 = 1.52 \times 10^{-7}$ s, 3.0×10^{-6} s for **1** and **2**, respectively. In view of the M versus H plots, it is clear that zero-field quantum tunnelling of magnetization (QTM) operates in complexes **2** and **3** while it is practically ineffective in complex **1**. This has been checked by measuring τ under dc fields for complexes **1** and **2**. Measurements at 3000 Oe yield an Arrhenius law characterized by different values of τ_0 (3.4×10^{-6} s) and Δ_{eff} (20.9 K) for the terbium complex **2**, which clearly indicate that the quantum relaxation pathway has been suppressed. At variance, the slight Δ_{eff} decrease observed for complex **1**, $\Delta_{eff} = 18.9$ K and $\tau_0 = 2.0 \times 10^{-7}$ s, does agree with a classical magnet behavior and confirms the absence of QTM for the $[LCoGdCoL]NO_3$ complex, **1**.

Mössbauer Spectroscopy

Mössbauer spectra have been recorded for the $[LFeLnFeL]ClO_4 \cdot CH_3OH$ complexes at 200, 80, and 5 K. The spectra at 200 and 80 K show a unique asymmetric quadrupole-split doublet while the spectra at 5 K exhibit more or less pronounced dipolar magnetic broadenings, Supporting Information, Figures S26 and S27. The asymmetry of quadrupole split doublets may stem from anisotropy of the recoilless fraction (Goldanskii−Karyagin effect),[42a] or from anisotropy of the populated magnetic states,[43] and/or to slow spin−spin relaxation of these magnetic states.[42b] Considering that (i) the two absorption lines of these asymmetric doublets have equal areas, and (ii) the asymmetry of the doublets does not increase with temperature (except for **9** where a minute increase, within statistical standard deviations, is observed), the first possibility was ruled out. On the other hand, considering that significant ferromagnetic interactions operate between Fe^{II} and Ln^{III} cations in complexes **8**−**10**, it may be viewed that these interactions are

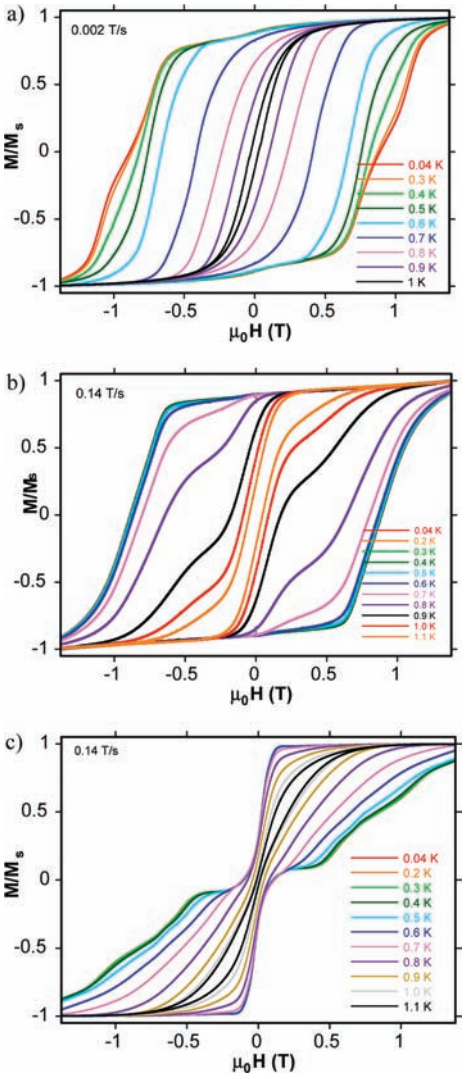

Figure 5. Magnetization M versus applied dc field H hysteresis loops for single crystals of **1** $[LCoGdCoL]NO_3$ (top), **2** $[LCoTbCoL]NO_3$ (middle), and **3** $[LCoDyCoL]NO_3.CH_3OH$ (bottom), at the indicated temperatures. The magnetizations are normalized to their saturation values M_S at 1.4 T.

(41) Wernsdorfer, W.; Chakov, N. E.; Christou, G. *Phys. Rev.* **2004**, *B 70*, 132413.

(42) (a) Greenwood, N. N.; Gibbs, T. C. *Mössbauer Spectroscopy*; Chapman and Hall: New York, 1971; pp 74−76. (b) Greenwood, N. N.; Gibbs, T. C. *Mössbauer Spectroscopy*; Chapman and Hall: New York, 1971; pp 72−74. (c) Greenwood, N. N.; Gibbs, T. C. *Mössbauer Spectroscopy*; Chapman and Hall: New York, 1971; pp 50−53.

(43) Borer, L.; Thalken, L.; Ceccarelli, C.; Glick, M.; Zhang, J. H.; Reiff, W. M. *Inorg. Chem.* **1983**, *22*, 1719.

Table 2. Mössbauer Parameters for Complexes $[LFeGdFeL]ClO_4$, **8**, $[LFeTbFeL]ClO_4 \cdot CH_3OH$, **9**, $[LFeDyFeL]ClO_4 \cdot CH_3OH$, **10**, and $[LFeLaFeL]ClO_4 \cdot CH_3OH$, **11**

	200 K				80 K			
complex	δ/mm cm^{-1}	ΔE_Q/mm cm^{-1}	Γ_+/mm cm^{-1}	Γ_-/Γ_+	δ/mm cm^{-1}	ΔE_Q/mm cm^{-1}	Γ_+/mm cm^{-1}	Γ_-/Γ_+
8 (FeGdFe)	1.097(9)	3.90(2)	0.16(1)	1.7(2)	1.10(1)	4.01(2)	0.17(1)	2.0(2)
9 (FeTbFe)	1.077(6)	3.93(1)	0.146(9)	1.23(8)	1.127(4)	3.978(7)	0.155(6)	1.17(5)
10 (FeDyFe)	1.085(6)	3.92(2)	0.155(7)	1.73(9)	1.15(2)	3.96(4)	0.26(2)	2.8(2)
11 (FeLaFe)	1.076(5)	3.802(9)	0.162(8)	1.21(6)	1.138(4)	3.857(8)	0.163(7)	1.34(6)

strong enough to create a preferred direction for S_z. However, it must be noticed that a similar but weaker asymmetry is observed for **11**, where no magnetic interactions operate between Fe^{II} and La^{III}. In view of these observations and comments, the Γ values of the Lorentzian lines in each doublet were allowed to vary independently during the fitting procedure. The Mössbauer parameters resulting from the fitting of such asymmetric doublets to the 200 and 80 K spectra of the four complexes are collated in Table 2. The derived isomer shift values, δ, close to 1.1 mm s^{-1}, are in agreement with high−spin iron(II) sites. They slightly decrease with increasing temperature, indicating operation of second-order Doppler effect.[42c] The quadrupole splittings, ΔE_Q, are close to the maximum value of 4 mm s^{-1}, and practically constant in the 80−200 K temperature range. Such large and temperature-independent quadrupole splittings imply that the ground state is an orbital singlet and that the energy separation between the ground state and the higher orbital states is very large, that is, the ligand field distortion of the octahedral symmetry has a strong axial component in all four [LFeLnFeL] complexes.

Discussion

Whatever the 3d/4f ratio used for synthesis, the complexes isolated with the nonadentate ligand L^{3-} are trinuclear 3d−4f−3d species, assembling two octahedral $[LM_{3d}]^-$ units through the 4f ion. The Co^{II}, Fe^{II} and Mn^{II} complexes reported here were prepared in a glovebox. While their solutions are air-sensitive, the isolated [LMLnML]X crystals are stable in the open atmosphere. The six methoxy groups of the two anionic $[LM]^-$ ligand complexes play an important function in preventing the unique counteranion, X^- (NO_3^- or ClO_4^-) from entering the 4f coordination sphere. The net result is that the entire set of complexes synthesized according to this experimental process are linear, with 3d−4f−3d angles comprised between 176.9(1) and 178.7(1)°, regardless of the counterion. The structures should be compared with those of the related complexes without 3-methoxy groups. When $[Ni(H_{1.5}L')]Cl_{0.5}$ (H_3L' = 1,1,1-tris[(salicylideneamino)methyl]ethane)) was allowed to react with $Ln^{III}(NO_3)\cdot 6H_2O$ in the presence of triethylamine (2:1:4 ratio), heterotrinuclear $[(L'Ni)_2Ln(NO_3)]$ complexes were obtained, in which a nitrate ion coordinates to the central Gd^{III} as a bidentate *O,O′*-chelate. The Ni···Ln···Ni angle is bent (ca. 140°) because of chelation of the NO_3^- ion.[8−10]

The synthesis of enantiopure compounds is of prime importance in several domains of chemistry. In organic chemistry, the problem of chirality is mainly directed toward the tetrahedral carbon atoms which can generate enantiomeric entities. In coordination chemistry, the stereochemistry of octahedral coordination complexes is also an important topic, since the genesis of coordination theory and Werner's work.[44] Indeed, the octahedron is the dominating coordination geometry in inorganic (stereo)chemistry. It has been shown that 144 "edge configurations" may be obtained for the octahedron by using different ligands, from monodentate to polydentate ones.[45,46] Among these 144 configurations, 72 are chiral, yielding helical structures represented by the Greek descriptors Δ and Λ. In the present case, reaction of the tame molecule (1,1,1-tris(aminomethyl)ethane) with *o*-vanillin yields a potentially nonadentate ligand able to coordinate a 3d ion in its inner N_3O_3 site. Once coordinated, this achiral ligand, which can be assimilated to the edge configuration number 15,[45] induces helicity around the metal ion, as a result of its screw arrangement. It is worth noting that only *fac* arrangements are possible, namely, *fac*-Λ and *fac*-Δ. Overwhelmingly, such complexes crystallize in centrosymmetric space groups, yielding a racemate in which the Δ and Λ enantiomers are present within each crystal, in a 1:1 ratio. In very few cases, however, conglomerates made of crystals containing homochiral complexes are obtained. Such an interesting example has been previously described by three of us. Deprotonation of $[Fe^{II}H_3L^2]^{2+}$ complexes (H_3L^2 = tris{[2-{(imidazole-4-yl)methylidene}amino]ethyl}-amine) yielded $[Fe^{III}L]$ complexes. These two building units form hexamer entities made of three $[Fe^{II}H_3L]^{2+}$−$[Fe^{III}L]$ pairs that self-assemble to produce extended homochiral 2D sheets held together by imidazole−imidazolate hydrogen bonds. Such sheets of identical chirality are packed together yielding a homochiral crystal (conglomerate). Circular dichroism spectra obtained from selected crystals confirmed that spontaneous resolution has occurred.[47]

In the present work, two hexacoordinate cobalt(II), manganese(II), or iron(II) complexes are assembled by the lanthanide ions to yield heterotrinuclear $[LCoLnCoL]NO_3$, $[LMnLnMnL]NO_3$, and $[LFeLnFeL]ClO_4$ complexes, respectively. In all cases, the isolated crystals do correspond to the homochiral $\Lambda-\Lambda$ and $\Delta-\Delta$ pairs, and the heterochiral $\Lambda-\Delta$ pair has never been obtained. Very recently a trinuclear $[L^1CoGdCoL^1]ClO_4$ complex prepared from a phosphorus-based tris hydrazone ligand, H_3L^1 (the H_3L^1 ligand was obtained by condensation of *o*-vanillin and (S)P[N(Me)-$NH_2]_3$) has been reported.[16a] In our study, the H_3L ligand is built by reacting 1,1,1-tris(aminomethyl)ethane (tame) instead of the hydrazone molecule with *o*-vanillin. Both ligands, H_3L^1 and H_3L, have nine coordination sites, but

(44) Werner, A. *Ber*. **1911**, *44*, 1887–1898. Werner, A. *Ber*. **1912**, *45*, 121–130.

(45) von Zelewsky, A. *Stereochemistry of Coordination Compounds*; Wiley: Chichester, 1996.

(46) Brorson, M.; Damhus, T.; Schäffer, C. E. *Inorg. Chem*. **1983**, *22*, 1569–1573.

(47) (a) Sunatsuki, Y.; Ikuta, Y.; Matsumoto, N.; Ohta, H.; Kojima, M.; Iijima, S.; Hayami, S.; Maeda, Y.; Kaizaki, S.; Dahan, F.; Tuchagues, J. P. *Angew. Chem., Int. Ed*. **2003**, *42*, 1614–1618. (b) Sunatsuki, Y.; Ohta, H.; Kojima, M.; Ikuta, Y.; Goto, Y.; Matsumoto, N.; Iijima, S.; Akashi, H.; Kaizaki, S.; Dahan, F.; Tuchagues, J. P. *Inorg. Chem*. **2004**, *43*, 4154–4171.

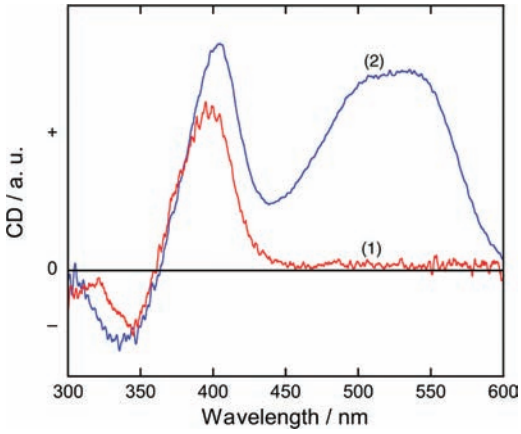

Figure 6. CD spectra of (1) [LMnTbMnL]NO_3 **6** and (2) [LFeTbFeL]$ClO_4 \cdot CH_3OH$ **9** in KBr disks, both complexes having the Λ−Λ configuration.

they differ by their capping tripods. Indeed the P−N bonds are longer than the corresponding C−C bonds by 0.1−0.14 Å while the N−N bonds are shorter than the C−N bonds by only 0.02−0.03 Å. Although the cobalt and gadolinium coordination spheres have very similar bond lengths in the two complexes, **1** and [L^1CoGdCoL^1]ClO_4, an important difference is observed. The phosphorus-based ligand induces a heterochiral pair, *fac*-Λ−Δ isomer, which crystallizes in the $P\bar{1}$ space group, while a homochiral pair, including *fac*-Λ−Λ and *fac*-Δ−Δ isomers, is observed in our equivalent [LCoGdCoL]NO_3 complex. The situation is even more interesting for the [LMnLnMnL]NO_3 complexes **5**, **6**, and **7**, the [LFeLnFeL]ClO_4 complexes **8**, **9**, **10**, and [LCoDyCoL]$NO_3 \cdot CH_3OH$, **3**, which do crystallize as conglomerates in the chiral $P2_12_12_1$ space group, yielding well separated *fac*-Λ−Λ and *fac*-Δ−Δ enantiomers. The circular dichroism spectra of complexes **6**, [LMnTbMnL]NO_3, and **9**, [LFeTbFeL]$ClO_4 \cdot CH_3OH$, recorded in the solid state, show positive (ca. 400 nm) and negative (ca. 340 nm) CD in the region of the Schiff base $\pi-\pi^*$ transition (Figure 6). Exciton theory[32] has been applied to tris(chelate)- or *cis*-bis(chelate)-type metal complexes, where chelate denotes such ligands as 2,2-bipyridine, 1,10-phenanthroline, or Schiff-base ligands, and the relationship between the CD pattern in the ligand $\pi-\pi^*$ transition region and the absolute configuration around the metal ion has been established. On the basis of exciton theory, we can assign the Λ−Λ configuration to the crystals of complexes **6** and **9**, whose CD spectra are described above. This assignment agrees with the X-ray crystallographic study. In spite of numerous trials, we have not been able to find a crystal corresponding to the Δ−Δ pair. This point deserves additional investigation regarding the possibility of total spontaneous resolution, where exclusive isolation of one of the enantiomers is achieved.[48] The cobalt case is more complicated, for [LCoDyCoL]$NO_3 \cdot CH_3OH$, **3**, is the only one among the [LCoLnCoL]NO_3 complexes crystallizing in the chiral $P2_12_12_1$ space group. Complexes, [LCoGdCoL]NO_3, **1**, and [LCoTbCoL]NO_3, **2**, crystallize in the $C2/c$ centrosymmetric space group, with Λ−Λ and Δ−Δ pairs coexisting in the crystal (racemic crystal). The counteranions, nitrate or perchlorate, do not play a prominent role for they are pushed out of the metal coordination spheres and not involved in hydrogen bonds. This may explain why most complexes in the present series crystallize in the same chiral space group, $P2_12_12_1$ irrespective of the nature of the counteranion. From the presently reported results it seems that the main factor responsible for the crystallization in chiral space groups is the size of the cations, mainly the 3d ones, the larger Mn^{II} and Fe^{II} cations yielding in this respect better results than the smaller Co^{II} cation.[49]

From the magnetic study, it seems clear that the larger deviations from the octahedron for the Fe complexes **8**−**11** induce quenching of the orbital contribution, as previously observed.[36,6] Consequently, a nice fit of the $\chi_M T$ versus T data (Figure 4c) is obtained by using an isotropic Hamiltonian. As expected from previous results dealing with Co−Gd or Fe−Gd complexes, the magnetic interactions governing the trinuclear complexes **1** and **8** are ferromagnetic in nature. The [LMnGdMnL]NO_3 complex **5** shows a similar behavior, except that the J constant (0.08 cm^{-1}) is much smaller than in the Co (0.52 cm^{-1}) and Fe (0.69 cm^{-1}) trinuclear entities. This difference cannot be explained by the number of electrons or pathways involved in the superexchange, respectively five, four, and three for Mn, Fe and Co complexes. This weak Mn−Gd ferromagnetic interaction is in good agreement with previous results on acetato bridged Mn−Gd complexes.[50] The large ZFS parameter D (around 6−7 cm^{-1}) obtained when fitting the two [LFeLnFeL] complexes **8** and **11** (Ln = Gd, La) agrees quite well with the large distortion from the octahedron toward the trigonal prism evidenced by the molecular structures of **8**, **9**, and **10**. The strong axial elongation component of this distortion which is suggested by the large D value is corroborated by the large and temperature-independent quadrupole splitting values, $\Delta E_Q \sim 4$ mm s^{-1}, derived from the Mössbauer spectra of all four [LFeLnFeL] compounds. These results imply that the ground state is an orbital singlet and that the energy separation between the ground state and the higher orbital states is large. The more or less pronounced dipolar magnetic broadenings evidenced in the spectra of **8**, **9**, and **10** at 5 K indicate operation of an internal magnetic field at the iron nuclei of these [LFeLnFeL] species. Considering that the molecular structures evidence well isolated [LFeLnFeL]$^+$ cations, these Zeeman spectra can not be related to long-range magnetic ordering. The ^{57}Fe Mössbauer spectra of high-spin ferrous compounds usually exhibit fast spin relaxation even at liquid helium temperatures, and in such a case quadrupole-split doublets are observed. However, slow paramagnetic relaxation effects have been observed in the spectra of a number of high-spin ferrous compounds.[51] The magnetic spectra due to

(48) Jacques, J.; Collet, A.; Wilen, S. H. *Enantiomers, Racemates and Resolutions*; Krieger Publishing Co: Malabar, FL, 1991.

(49) Huheey, J. E. *Inorganic Chemistry*; Harper § Row Publishers: New York, 1978.

(50) Prasad, T. K.; Rajasekharan, M. V.; Costes, J. P. *Angew. Chem., Int. Ed.* **2007**, *46*, 2851–2854.

(51) (a) Ok, H. N. *Phys. Rev.* **1969**, *185*, 472–476. (b) Petrouleas, V.; Simopoulos, A.; Kostikas *Phys. Rev. B.* **1975**, *12*, 4675–4681. (c) Price, D. C.; Johnson, C. E.; Marteense, I. *J. Phys. C: Solid State Phys.* **1977**, *10*, 4843–4854. (d) Nicolini, C.; Reiff, W. M. *Inorg. Chem.* **1980**, *19*, 2676–2679. (e) Srivastava, K. K. P. *J. Phys. C: Solid State Phys.* **1983**, *16*, L53–L55. (f) Charron, F. F.; Reiff, W. M. *Inorg. Chem.* **1986**, *25*, 2786–2790. (g) Howes, B. D.; Creagh, D.; Price, D. C. *J. Phys. C: Solid State Phys.* **1988**, *21*, 2439–2452. (h) Garge, P.; Chikate, R.; Padhye, S.; Savariault, J.-M.; de Loth, P.; Tuchagues, J.-P. *Inorg. Chem.* **1990**, *29*, 3315–3320. (i) Martinez Lorente, M. A.; Dahan, F.; Petrouleas, V.; Bousseksou, A.; Tuchagues, J.-P. *Inorg. Chem.* **1995**, *34*, 5346–5357. (j) Reiff, W. M.; LePointe, A. M.; Witten, E. H. *J. Am. Chem. Soc.* **2004**, *126*, 10206–10207.

paramagnetic relaxation are related with non-Kramer's doublets exhibiting a significant Ising type anisotropy. The magnetically split spectra at zero external magnetic field are due to mixing between the electronic and nuclear spin states.[52] In assessing the origin of the slow magnetic relaxation in **8**, **9**, and **10** one might readily argue that the relatively high effective spin of their ground state in combination with a high uniaxial magnetoanisotropy could lead to an SMM behavior.[53] However, the experimental data do not evidence clearly (**9**) or at all (**8**, **10**) an SMM behavior: this may be related to the possibility that 3d and 4f anisotropies can have additive or subtractive effects and/or to particularly efficient zero-field quantum tunnelling of magnetization (QTM) in the ferrous derivatives.

We have previously shown that the SMM property of a heterodinuclear Cu−Tb complex was a property characteristic of the Cu−Tb pair, and could not be attributed to the Tb ion alone.[54] This result demonstrated that the presence of a paramagnetic ion (here Cu^{II}) interacting with a Tb ion was able to increase the magnetic anisotropy of the resulting system. This observation suggested a way for increasing the SMM property through replacement of copper by a more anisotropic d ion such as cobalt. The present work develops this idea. The large separation of the heterotrinuclear molecules, because of the methoxy groups of the main ligand, implies that the observed SMM behavior is an intramolecular property. The absence of such a behavior in complexes **4**, $[LCoLaCoL]NO_3 \cdot CH_3OH$, **12**, $[LZnTbZnL]NO_3 \cdot 3H_2O$, and **13**, $[LZnDyZnL]NO_3 \cdot 2H_2O$, allows us to confirm that the out-of-phase ac magnetic component observed in complexes **1**, **2**, and **3** is a property characteristic of the Co−Gd−Co, Co−Tb−Co, and Co−Dy−Co triads, and cannot be attributed to the Co, Tb, or Dy ions alone.

It has been recently shown in literature that trinuclear $[L^1CoGdCoL^1]ClO_4$ complexes[16a] including a phosphorus-based tripodal ligand similar to L, behave as SMM molecules. Although ac-measurements suggest SMM behavior, the observation of out of phase susceptibility signals χ'' cannot prove it. By performing hysteresis loop measurements, we clearly prove for the first time the SMM behavior of our complexes involving cobalt and lanthanide ions, $[LCoGdCoL]NO_3$ **1**, $[LCoTbCoL]NO_3$ **2**, and $[LCoDyCoL]NO_3 \cdot CH_3OH$ **3**. Indeed, large hysteresis loops are observed in the three cases, with coercive fields of 8860, 7330, and 4900 Oe for **1**, **2**, and **3**, respectively. Among them, the $[LCoGdCoL]NO_3$ complex **1** seems to appear as the most performing for it is devoid of quantum relaxation pathway at $H = 0$ Oe. Unfortunately, this phenomenon is not reproduced in the equivalent Fe^{II}-Ln complexes and, less surprisingly, in the Mn^{II}-Ln complexes where anisotropy is brought by the sole Ln ions.

Conclusion

The use of an original tripodal and trianionic nonadentate ligand yielded, under controlled atmosphere, trinuclear 3d−4f−3d complexes (3d = Mn^{II}, Fe^{II}, Co^{II}, Zn^{II} and 4f = La^{III}, Gd^{III}, Tb^{III}, Dy^{III}) whatever the 3d/4f synthetic ratio. The methoxy groups participate, as expected, in weak O−Ln bonds, but, in addition, they have a major role in preventing the unique counteranion, X^- (NO_3^- or ClO_4^-) from entering the 4f coordination sphere, thus orienting the reactions toward linear face-sharing heterotrinuclear 3d−4f−3d species. The magnetic interactions governing these trinuclear complexes are ferromagnetic in nature and characterized by larger M−Gd interaction parameters for Co^{II} (0.52 cm^{-1}) and Fe^{II} (0.69 cm^{-1}) than for Mn^{II} (0.08 cm^{-1}). Quenching of the orbital contribution, induced by the large deviations from the octahedron geometry, is more efficient in the Fe complexes than in the Co entities. The large ZFS parameters D (around 6−7 cm^{-1}) obtained when fitting the Fe complexes result from the strong axial elongation of their coordination sphere; these values are corroborated by the large temperature-independent quadrupole splitting values, $\Delta E_Q \sim 4$ mm s^{-1}, derived from their Mössbauer spectra. From a structural point of view, complexation of the achiral L ligand induces helicity around the 3d ion and facial arrangements. Assembling two 3d complexes by Ln ions yields homochiral Λ−Λ, Δ−Δ molecules, the heterochiral Λ−Δ molecules being never observed. Racemate crystals are obtained when cobalt ions are associated to Gd or Tb but conglomerates are obtained for the entire set of Mn and Fe complexes, along with the cobalt−dysprosium species. This implies occurrence of spontaneous resolution as confirmed by the solid-state circular dichroïsm spectra of the later complexes. We have also demonstrated that some of these trinuclear complexes are single-molecule magnets. Among them, the cobalt-Ln complexes have the more interesting magnetic properties: they exhibit large magnetization hysteresis loops evidenced for the first time in Co−Ln species. The higher energy barrier for the reversal of magnetization is obtained for complex **1**, $[LCoGdCoL]NO_3$, as a consequence of the absence of zero-field QTM. The strategy consisting in selecting the more anisotropic ions in 3d−4f complexes has been successful with Co^{II}, but not with Fe^{II}, suggesting thus that 3d and 4f anisotropies can have additive or subtractive effects, according to the geometries of the resulting complexes. Zero-field quantum tunnelling of magnetization (QTM) is another factor which possibly plays a role in this difference of behavior. Further work is in progress to better understand these phenomena and also to synthesize new chiral SMMs.

Supporting Information Available: Tables S1−S4, Figures S1−S27, and crystallographic data in CIF format. This material is available free of charge via the Internet at http://pubs.acs.org.

(52) Surerus, K. K.; Hendrich, M. P.; Christie, P. D.; Rottgardt, D.; Orme-Johnson, W. H.; Münck, E. *J. Am. Chem. Soc.* **1992**, *114*, 8579–8590.
(53) (a) Boudalis, A. K.; Clemente-Juan, J. M.; Sanakis, Y.; Mari, A.; Tuchagues, J.-P. *Eur. J. Inorg. Chem.* **2007**, 2409–2415. (b) Boudalis, A. K.; Sanakis, Y.; Clemente-Juan, J. M.; Donnadieu, B.; Nastopoulos, V.; Mari, A.; Coppel, Y.; Tuchagues, J.-P.; Perlepes, S. P. *Chem.—Eur. J.* **2008**, *14*, 2514–2526.
(54) Costes, J. P.; Dahan, F.; Wernsdorfer, W. *Inorg. Chem.* **2006**, *45*, 5–7.